

# In situ investigation of phosphonate retarder interaction in oil well cements at elevated temperature and pressure conditions

Kunal Kupwade-Patil<sup>1</sup>  | Peter J. Boul<sup>2</sup> | Diana K. Rasner<sup>2</sup> | Saul H. Lapidus<sup>3</sup> | Juscelino B. Leao<sup>4</sup> | Kenneth D. Johnson<sup>2</sup> | Carl J. Thaemlitz<sup>2</sup> | Oral Büyüköztürk<sup>1</sup> 

<sup>1</sup>Laboratory for Infrastructure Science and Sustainability (LISS), Department of Civil and Environmental Engineering, Massachusetts Institute of Technology, Cambridge, MA, USA

<sup>2</sup>Aramco Research Center (ARC), Houston, TX, USA

<sup>3</sup>X-ray Science Division, Advanced Photon Source, Argonne National Laboratory, Lemont, IL, USA

<sup>4</sup>NIST Center for Neutron Research (NCNR), National Institute of Standards and Technology, Gaithersburg, MD, USA

## Correspondence

Oral Büyüköztürk, Department of Civil and Environmental Engineering, Massachusetts Institute of Technology, Cambridge, MA 02139, USA.

Email: obuyuk@mit.edu

## Funding information

Aramco Services Company; US Department of Energy, Grant/Award Number: DE-AC02-06CH11357; National Science Foundation, Grant/Award Number: DMR-1419807

## Abstract

The effect of a high-performance retarding additive in oil well cements was investigated under elevated temperature (165°C) and pressure (1000 psi) conditions via in situ synchrotron-based X-ray diffraction (XRD) and quasielastic neutron scattering (QENS) techniques. Under these temperature and pressure conditions, crystalline calcium silicate hydrates (C–S–H) are formed through the cement hydration process. From in situ XRD experiments, the retardation effect was observed by a change in the rate of the appearance of 11 Å tobermorites as well as a change in the rate of the  $\alpha$ -C<sub>2</sub>SH generation and depletion. QENS analysis revealed that the retardation effect was related to the non-conversion of free water to chemical and constrained water components. A high presence of free water components was attributed to a decrease in 11 Å tobermorites along with slower consumption of the quartz and portlandite phases. Furthermore, QENS results infer that the water molecules experienced confinement in the restricted pore spaces. The retarder inhibited this initial water confinement by slowing the bulk diffusion of free water in the confined region.

## KEYWORDS

neutron scattering, oil well cements, retarders, synchrotron X-ray diffraction

## 1 | INTRODUCTION

Oil and gaswell cements must be designed with favorable, low viscosities for placement within wells and high strengths of set cements after placement. Failure to engineer oil well cements appropriately can lead to loss of zonal isolation, which in turn leads to environmental hazards, losses in production, and safety-related issues.<sup>1</sup> Well cements are engineered using chemical additives to achieve desirable mechanical strength by governing the rheological properties, fluid loss control, and setting time of the cement slurry. In addition to exposure to severe temperature and pressure conditions, cements must also be designed to resist corrosive

fluids and pressurized formation fluids.<sup>2</sup> Chemical additives can tailor the well cements to accommodate these aggressive conditions by modifying the behavior of the hydrating cement paste. Chemical additives are categorized as accelerators, retarders, extenders, weighting agents, dispersants, fluid-loss control agents, and special additives.<sup>2</sup> Accelerators are used in cement slurries to reduce the setting time of hydration by speeding the hardening process. In contrast, the role of retarders is to delay the setting of the cement slurries and likewise delay mechanical strength development of the cementitious binder. Each specific retarder can have a significant impact on the induction period and can alter the complex reaction mechanism.<sup>3–6</sup>

A complete understanding of chemical reactions and microstructural development during the hydration process of oil well cement slurries with additives is necessary for designing oil well cements under downhole conditions. Time-resolved X-ray and neutron scattering techniques are helpful in deciphering these complex reactions by providing an in-depth insight into the resulting microstructure and dynamics of the hydrating cement paste. These in situ techniques allow insights into the cement hydration process by simulating the actual downhole environment through the application of appropriate pressure and temperature conditions. High-energy X-ray diffraction (XRD) using a synchrotron facility has been previously used to examine the effect of retarding additives on Class H and Class G oil well cements.<sup>7-10</sup> High-energy X-rays have a higher sample penetration capacity compared to laboratory diffractometers, thus eliminating absorption and fluorescence-related problems. The shorter wavelength of the synchrotron X-ray beam provides enhanced structural information about the sample by enabling wider scattering vector ( $Q$ ) for smaller d-spacing. The extremely high-flux and high-resolution data permit a greater number of peaks to be resolved, which is essential for correct pattern indexing. Therefore, synchrotron-based XRD is useful to precisely detect the evolution of phases during cement hydration.

An understanding of cement chemistry is required to decipher the effect of additives on the phase evolution during the oil well cement hydration process. During hydration under ambient conditions, tri-calcium silicate ( $C_3S$ ) and di-calcium silicate ( $C_2S$ ) produce semi-amorphous calcium silicate hydrate ( $C-S-H$ ) and a crystalline form of calcium hydroxide, known as portlandite. However, under higher temperature conditions, an increase in the Ca/Si ratio is observed in the formation of different crystalline forms of  $C-S-H$ , such as jaffeite,  $Ca_6[SiO_7](OH)_6$  and  $\alpha-C_2SH$ ,  $[Ca_2(HSiO_4)(OH)]$ .<sup>11</sup> Formation of jaffeite and  $\alpha-C_2SH$  is known to lead to a detrimental effect on the mechanical strength of the cement slurries. At 160°C, with additional pressure applied, jaffeite converts to  $\alpha-C_2SH$ .<sup>12</sup> The Ca/Si ratio is reduced by including additional siliceous material which results in the formation of tobermorites. The tobermorite group mainly consists of 14 Å tobermorite,  $Ca_5Si_6O_{16}(OH)_2 \cdot 7H_2O$  or plombierite, 11 Å tobermorite,  $Ca_4Si_6O_{15}(OH)_2 \cdot 5H_2O$ , and 9 Å tobermorite,  $Ca_5Si_6O_{16}(OH)_2$  or riversideite. Between 80°C and 100°C, 14 Å tobermorite transforms to 11 Å tobermorite, while at 300°C it further reduces to 9 Å tobermorite, and above 800°C it recrystallizes to wollastonite,  $Ca_3Si_3O_9$ . Above 150°C tobermorites can gradually change into xonotolite,  $Ca_6Si_6O_{17}(OH)_2$ , and gyrolite.<sup>11</sup> Elevated pressure conditions can expedite the growth of tobermorites; however, it is still unclear why pressure has such a prominent effect on the hydration process.<sup>7</sup> In addition to microstructure analysis via XRD, an examination of reaction kinetics is required to evaluate the conversion of free water to bound water throughout

the course of hydration. Tracking water dynamics is an indirect measure of setting time, which is an essential parameter for assessing the additive effect in oil well cementing. In situ quasielastic neutron scattering (QENS) is a powerful tool, which can be used to examine hydration behavior by simulating downhole conditions. QENS facilitates quantification of various H/H<sub>2</sub>O environments by evaluating free, constrained, and chemically bound (CB) H-atoms. QENS has widely been used to study the hydration process of  $C-S-H$ ,<sup>13-19</sup> portland cement paste with natural<sup>20</sup> and nano-additives,<sup>21</sup> geopolymer cements,<sup>22</sup> and alkali-activated binders.<sup>23</sup> The QENS data have been used to model the nucleation and growth process by providing insight into the induction period of  $C_3S$  hydration.<sup>16</sup> Recently, reactive force dynamics was used to simulate reaction dynamics of water molecules confined inside the  $C-S-H$  nanopores.<sup>24</sup> These results demonstrate that the diffusion coefficients obtained from molecular dynamic simulations match well with QENS and nuclear magnetic resonance experiments.

The goal of the current work is to evaluate the effect of a phosphonate-based retarder on the hydration of oil well cements, considering both microstructure and water dynamics. To simulate downhole conditions, these in situ experiments were performed at elevated temperature and pressure conditions. The phase evolution and water dynamics were investigated via synchrotron-based XRD and QENS techniques. A new way to examine the impact of retarders on oil well cement hydration was proposed by considering both the water environment along with the microstructural phase evolution during the early stage of hydration. To our knowledge, this is the first in situ QENS experiment on oil well cements performed under elevated temperature and pressure conditions. This research is significant because it has the potential to provide new insights into effectively engineering additives in oil well cements by using accurate and real-time monitoring techniques.

## 2 | MATERIALS AND METHODS

### 2.1 | Raw material characterization and mixing

For in situ synchrotron XRD experiments, Class G cement powder was mixed with silica flour and was examined with and without diethylenetriamine penta (methylene phosphonic acid) DTPMP retarder. The samples with and without the DTPMP retarder were designated as Class G and Class G + R, respectively. For the Class G + R sample, 0.2 wt% of Class G cement was replaced by the DTPMP retarder. Since the DTPMP retarder was in a liquid form, it was mixed with water before combining it with the cement and silica flour. A water-to-cement ratio of 0.65 was used for both these

samples. Prior to inserting the samples into a capillary, a vortex mixer was used to ensure uniform mixing of the cement paste samples.

Two samples were run for QENS experiments. A three-retarder system was selected containing DTPMP, zinc oxide (ZnO), and an acrylic polymer (PCR-3), while the binder consisted of Class G cement and silica flour. Hydroxyethyl cellulose was used as a free water control additive. The control sample consisted of Class G cement and silica flour along with the cellulose organic polymer. The sample with three retarders was labeled as Class G + 3R, while the control sample without the retarder was designated as Class G. A water to cement ratio of 0.65 was used for these samples.

## 2.2 | High pressure/temperature setup for in situ synchrotron XRD experiments

The cement slurries for X-ray investigation were placed inside a triple-walled Kapton tube with an internal diameter of 1 mm. One end of the Kapton tube was sealed using 1/16-inch stainless Swagelok fittings with 1.2 mm ferrules. The other end was connected to a high-pressure pump, as shown in Figure 1. A pressure of 1000 psi was applied using a

high-pressure pump, and external hot blowers were used to heat the Kapton tube to 165°C. Thermocouples were used to monitor the temperature throughout the experiment.

The XRD data were collected at Beamline 11-BM at the Advanced Photon Source at Argonne National Laboratory. The X-ray wavelength was set to 0.41274 Å and a fixed energy of 30 keV was used for this experiment. Data were recorded at a temperature of 165°C and a pressure of 1000 psi with a  $2\theta$  range from 1° to 30° with a counting time of 10 minutes per scan. Samples were rotated at approximately 5800 rpm around the capillary axis for the first 5 minutes prior to the application of pressure and temperature on the sample. Data were collected while continually scanning the diffractometer  $2\theta$  arm. A mixture of National Institute of Standards and Technology (NIST) standard reference materials, Si (SRM 640c) and Al<sub>2</sub>O<sub>3</sub> (SRM 676), was used to calibrate the instrument, where the Si lattice constant determines the wavelength for each detector. Corrections were applied for detector sensitivity,  $2\theta$  offset, small differences in wavelength between detectors, and the source intensity, as noted by the ion chamber before merging the data into a single set of intensities evenly spaced in  $2\theta$ .

The phases were analyzed using HighScore Plus Software,<sup>25</sup> where the wavelength was set to 0.41274 Å

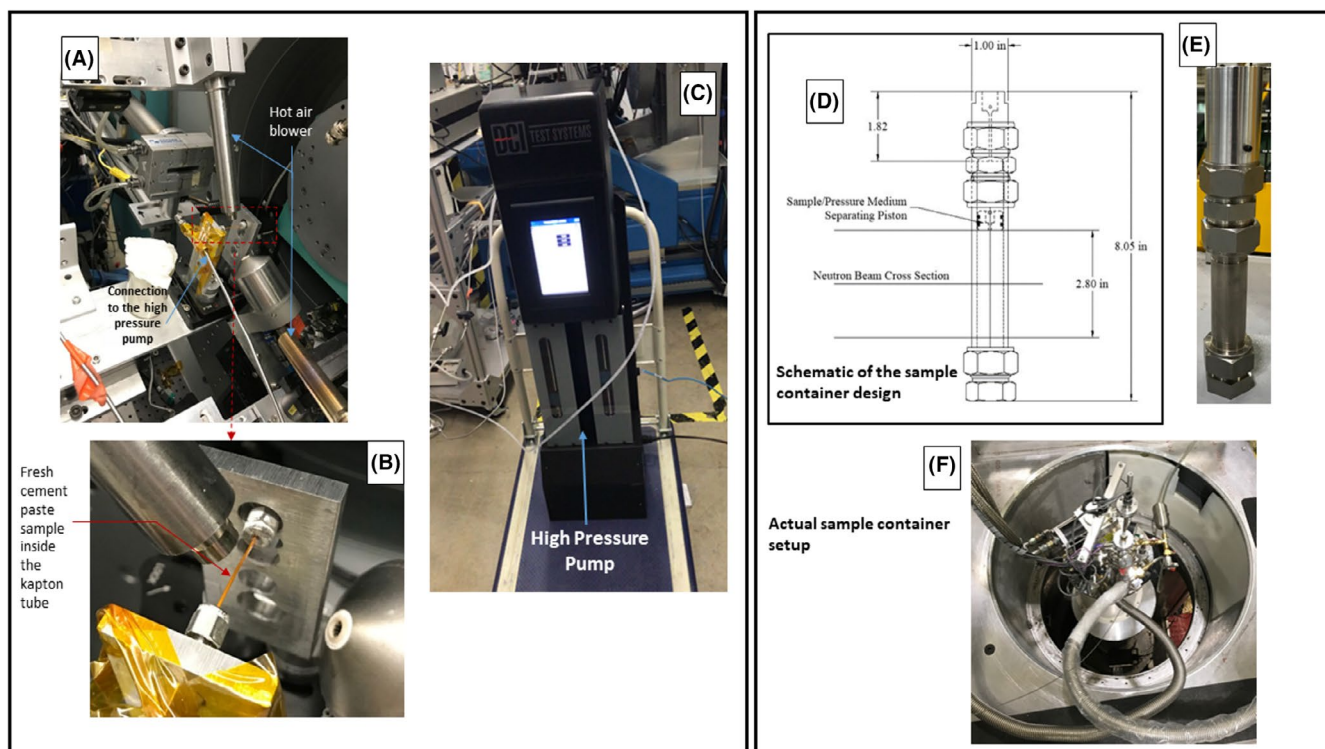


**FIGURE 1** A, Actual sample setup for performing elevated temperature (160°C) and pressure (1000 psi) experiment at Beamline 11-BM at the Argonne National Laboratory. B, Zoomed image showing the Kapton tube which consists of fresh cement paste and the blower. C, High-pressure pump used to apply 1000 psi pressure. D, Schematic diagram of the special annular pressure vessel designed and manufactured at the National Institute of Standards and Technology (NIST) Center for Neutron Research for cement samples which can withstand elevated temperature and pressure conditions (Image courtesy by Juscelino Leao). E, Actual mold filled with cement paste. F, Top loading of the sample mold inside the Disk Chopper Spectrometer at NIST [Color figure can be viewed at [wileyonlinelibrary.com](http://wileyonlinelibrary.com)]

before running the analysis. Note that the XRD data reported here were collected at a synchrotron facility at a fixed energy of 30 keV, whereas most XRD data reported in the literature use Cu K-alpha X-ray source with an energy of 8.04 keV and a wavelength of 1.5406 Å. Peaks related to these phases were integrated to give intensity vs time. The area under the peak was determined, which is taken to be proportional to its intensity. For example, quartz was identified, and the area was integrated to give the maximum values of the intensity.

### 2.3 | QENS experiments at elevated temperature and pressure conditions

Quasielastic neutron scattering experiments on hydrating cement pastes were performed using a disk chopper spectrometer (DCS) at the NIST Center for Neutron Research (NCNR). A unique annular titanium pressure vessel was used to perform this experiment as shown in Figure 1D. The total volume of the vessel was 80 mL. An insert was used to create a 1 mm annular space across the neutron beam path. Moreover, a piston was used to ensure hydrostatic pressure and to separate the sample from the pressure media. A pressure of 1000 psi was maintained throughout the experiment. A top-loading closed cycle refrigerator was used for this experiment, and the temperature on the

sample was increased using a heater on the sample stick. Furthermore, a temperature heat shield and a heat conduction strap were used to minimize the temperature gradient across the pressure vessel. High-temperature sensors were used to monitor the sample temperature throughout the hydration process. In addition to the pressure of 1000 psi, the cement paste samples were subjected to temperatures of 165°C. Two cement paste samples were measured with the retarder and control (without retarder) for 40 and 11.5 hours, respectively. The incident monochromatic neutron wavelength was 6.0 Å, which resulted in an energy resolution of full-width half maximum of about 64 μeV. The detectors were grouped to obtain a set of spectra in the Q range from 0.1–2 Å<sup>-1</sup>.

### 2.4 | Ultrasonic cement analyzer

All tests were carried out according to the American Petroleum Institute Recommended Practice 10B.<sup>26</sup> The pressure in all tests with the ultrasonic cement analyzer (UCA) was set to 1000 psi (6.89 MPa). The temperature ramps were set to move to the target temperatures within 1 hour. For all the samples, the target temperature was set to 165°C. The UCAs used were Chandler 4265 HT models manufactured by Chandler engineering in Broken Arrow, Oklahoma.

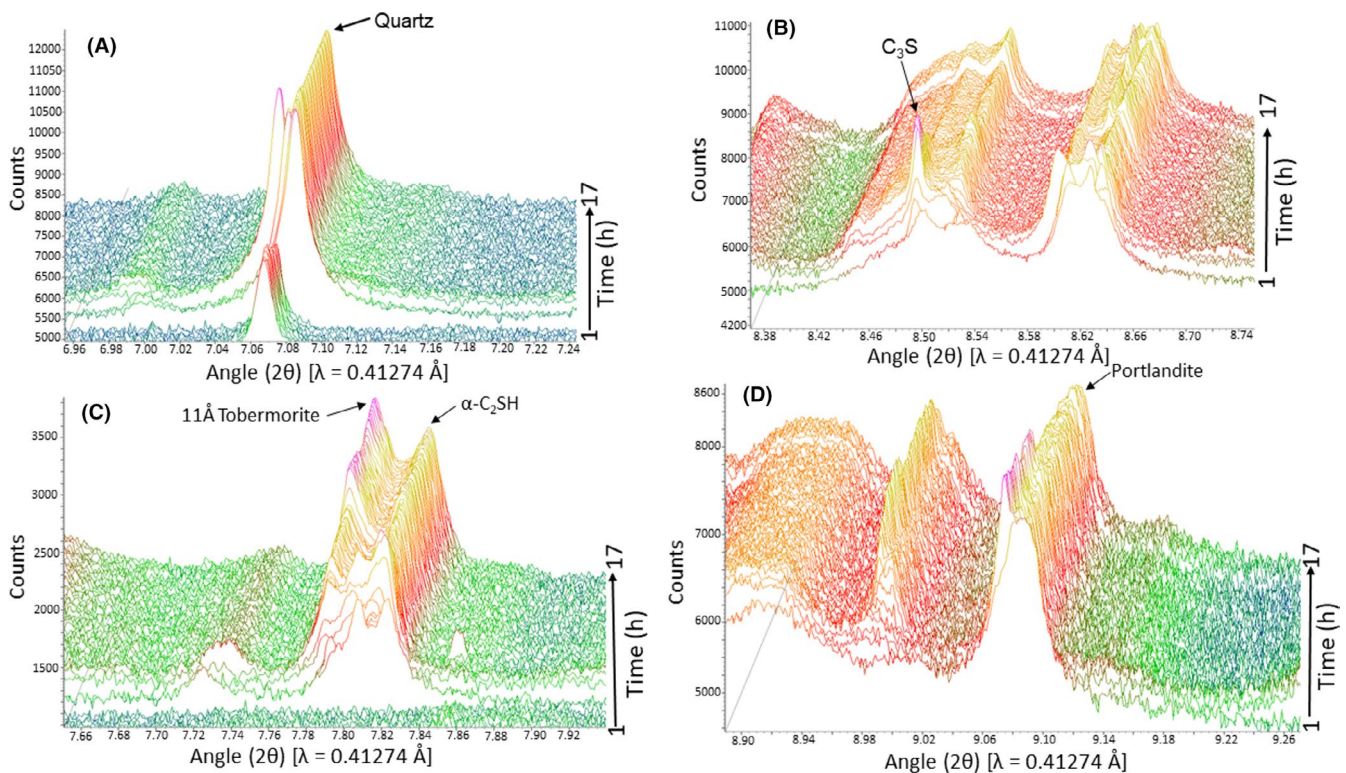


**FIGURE 2** Time-resolved in situ synchrotron X-ray diffraction data for hydrating Class G cement paste in (A) quartz, (B) C<sub>3</sub>S, (C) 11 Å tobermorite, and α-C<sub>2</sub>SH, and (D) portlandite phases [Color figure can be viewed at [wileyonlinelibrary.com](http://wileyonlinelibrary.com)]

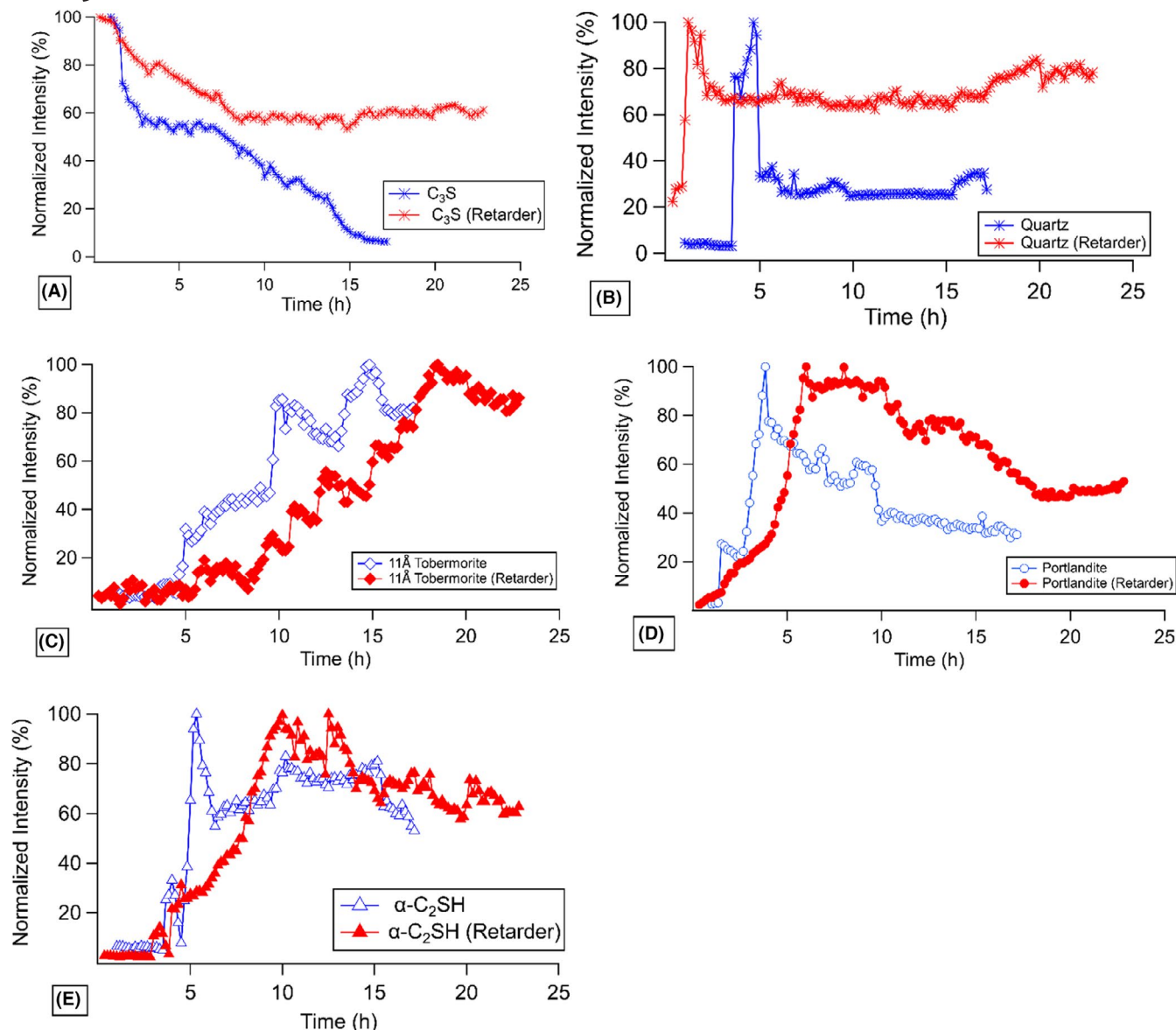


**FIGURE 3** Time-resolved phase concentration vs time plots for hydration experiments at a temperature of 160°C and pressure of 1000 psi. Each plot is normalized so that its maximum intensity is unity. Hydration path for (A)  $C_3S$ , (B) quartz, (C) 11 Å tobermorite, (D) portlandite, and (E)  $\alpha$ - $C_2SH$  for Class G cement with and without retarders [Color figure can be viewed at [wileyonlinelibrary.com](http://wileyonlinelibrary.com)]

### 3 | RESULTS AND DISCUSSION

In what follows, we describe the mineralogical information obtained by in situ diffraction measurements, where details related to the evolution of hydration products influenced by retarders are examined at elevated temperature and pressure conditions. This is followed by an investigation of water dynamics using QENS techniques to decipher the effect of phosphonate-based retarders on Class G oil well cements.

#### 3.1 | Synchrotron XRD

Time-resolved in situ XRD data for the Class G cement paste collected up to 17 hours are shown in Figure 2. The dominant

phases were quartz (International Centre for Diffraction Data [ICDD]: 01-070-3755),  $C_3S$  (ICDD: 01-070-8632),  $\alpha$ - $C_2SH$  (ICDD: 04-009-6343), 11 Å tobermorite (ICDD: 00-019-1364), and portlandite (ICDD: 00-004-0733); these are shown in Figure 2A-D. The XRD patterns from the ICDD database were used as a reference for data analysis. Using the ICDD reference patterns, the maximum intensity peak for quartz at 7.07°, portlandite at 9.00°, 11 Å tobermorite at 7.781°,  $\alpha$ - $C_2SH$  at 7.809°, and  $C_3S$  at 8.48° were detected. It is interesting to note that the maximum intensity peaks for 11 Å tobermorite and  $\alpha$ - $C_2SH$  peaks lie adjacent to each other, as shown in Figure 2C.

The progress of hydration paths for  $C_3S$ , quartz, 11 Å tobermorite, portlandite, and  $\alpha$ - $C_2SH$  is shown in Figure 3A-E, respectively. Peaks related to these phases were integrated

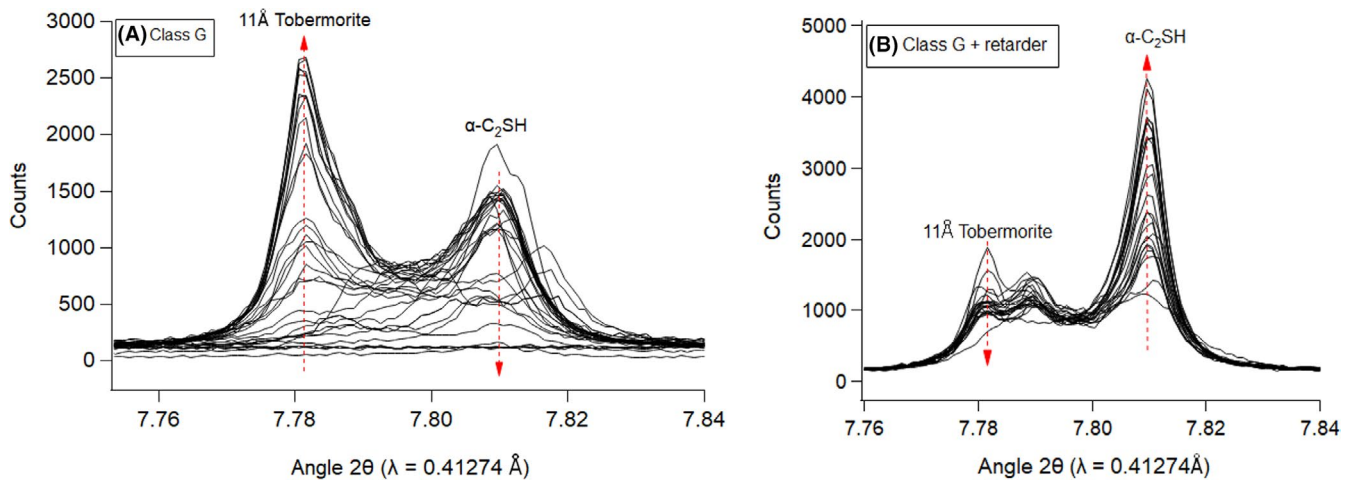


**FIGURE 4** Plot for (A) Class G cement and (B) Class G cement with retarder showing the effect of 11 Å tobermorite and  $\alpha$ -C<sub>2</sub>SH phase with the increase in hydration time (arrows represent the general trend for actual time stamp; refer to Figure 3) [Color figure can be viewed at [wileyonlinelibrary.com](http://wileyonlinelibrary.com)]

to give intensity vs time plots. In what follows, we investigate the effect of the retarder on each phase and its impact on other related phases.

### 3.1.1 | C<sub>3</sub>S

Normally during cement hydration the C<sub>3</sub>S phase gets consumed, producing C–S–H and a crystalline form of calcium hydroxide, which is portlandite.<sup>11</sup> For the Class G sample, the normalized intensity dropped by almost 60% at 2.2 hours, while a similar intensity value for the Class G + R sample was observed after 9 hours (Figure 3A). A decrease in the C<sub>3</sub>S phase was much faster in the Class G sample compared to the Class G + R sample, suggesting that the C<sub>3</sub>S phase is getting consumed in forming 11 Å tobermorite phase. The highly crystalline 11 Å tobermorite occurs typically at temperatures above 140°C and is predominantly responsible for the increase in strength.<sup>11</sup> C<sub>3</sub>S hydration above 160°C at elevated temperature/pressure conditions leads to  $\alpha$ -C<sub>2</sub>SH instead of jaffeite.<sup>27</sup> Therefore,  $\alpha$ -C<sub>2</sub>SH was observed in these samples, as shown in Figure 3E.

It is known that the termination of cement induction period is detected via the rapid formation of portlandite by increasing the rate of C<sub>3</sub>S consumption. This infers that the inclusion of a retarder facilitates slower consumption of C<sub>3</sub>S by arresting the early formation of portlandite.<sup>8,12</sup> Moreover, all retarders increase the time before the commencement of rapid hydration of C<sub>3</sub>S.<sup>8</sup> Therefore, the retardation possibly occurs through the stabilization of surface layers on the cement grains that prevent rapid ingress of water.<sup>3</sup> Retardation could occur through a multitude of processes, including calcium ion complexation influenced by Portlandite suppression, simultaneously delaying the conversion of free water to CB water in forming C–S–H-related phases.<sup>4</sup> In addition,

other related retardation mechanisms may be delaying the nucleation and growth of the hydrates.<sup>28</sup>

### 3.1.2 | Portlandite and quartz

The rapid near-term increase in the evolution of portlandite due to elevated pressure and temperature conditions was observed, as shown in Figure 3D. The Class G sample showed a steep rise in portlandite within the first 2 hours, whereas the Class G + R showed a gradual rise in portlandite. The retarder helped to delay the early rapid increase in portlandite, thus prolonging the induction period during the first few hours of hydration. The portlandite precipitation is suppressed, while slowing the C<sub>3</sub>S dissolution due to no changes in the degree of saturation, resulting in the delay in C–S–H precipitation, causing prolonged induction periods.<sup>29</sup> The Class G sample (control) showed a rapid decrease in portlandite after 4 hours of hydration compared to the Class G + R sample, which showed a gradual decrease in portlandite for up to 18 hours of hydration. The loss of portlandite at elevated temperature and pressure conditions has been attributed to the formation of high-temperature C–S–H-related phases, such as 11 Å tobermorite and  $\alpha$ -C<sub>2</sub>SH.<sup>7</sup> As the portlandite concentration drops, quartz begins to get consumed, as shown in Figure 3B. The silica flour was used to provide the high-temperature resistance to strength retrogression in the binder, which mostly comprises quartz. During the first 5 hours of hydration, a sharp spike in quartz was observed mostly due to the silica flour involvement in the hydration reaction. Besides, other unknown trace elements in the material may be responsible for the sharp increase in quartz. A study by Bresson et al shows that silicate chains of C–S–H-related phases, including 11 Å tobermorite, are attributed to the presence of quartz.<sup>27</sup> Here, the quartz consumption infers that

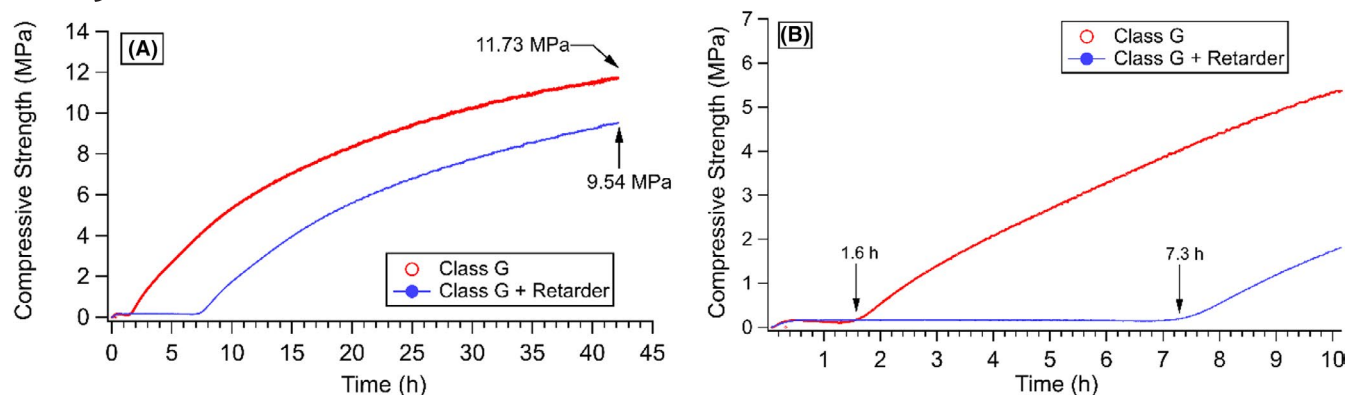


**FIGURE 5** Effect of a phosphonate retarder in Class G cement paste using an ultrasonic cement analyzer. A, Data from 0 to 43 h. B, Zoomed image for the data up to 10 h [Color figure can be viewed at [wileyonlinelibrary.com](http://wileyonlinelibrary.com)]

portlandite is dissolving into the pore solution and reacting with quartz from the silica flour. The decline in quartz and portlandite has been attributed to an increase in 11 Å tobermorite, while simultaneously decreasing the  $\alpha$ -C<sub>2</sub>SH phase (see Figures 3C,E and 4).

### 3.1.3 | 11 Å Tobermorite

A relation between quartz and 11 Å tobermorite could be established where consumption of quartz leads to an increase in 11 Å tobermorite. The Class G sample showed an early increase in the 11 Å tobermorite phase after approximately 5 hours of hydration with a jump in the normalized intensity from 50% to 100% between 2 and 8 hours of hydration (see Figure 3C). Simultaneously, depletion of quartz was detected between the range of 4 and 6 hours (see Figure 3B). The Class G + R sample indicated a slower rate of increase in the 11 Å tobermorite phase as compared to the Class G sample. In the presence of a retarder, less portlandite was consumed in relation to a slower 11 Å tobermorite rate of increase. A relation between the 11 Å tobermorite and  $\alpha$ -C<sub>2</sub>SH phases is shown in Figure 4. The 11 Å tobermorite formed in the Class G + R sample showed a double peak, suggesting that aluminum distribution among the tobermorite crystals may be bimodal because they gave rise to two peaks varying slightly in d-spacing due to variations in the alumina content.<sup>9</sup>

### 3.1.4 | $\alpha$ -C<sub>2</sub>SH

The  $\alpha$ -C<sub>2</sub>SH phase did not appear during the first 4 hours for the Class G sample. During the early stage of hydration, the Class G sample showed a drastic increase in  $\alpha$ -C<sub>2</sub>SH up to 5.2 hours of hydration, while the Class G + R sample showed a steady rise in  $\alpha$ -C<sub>2</sub>SH up to 10 hours. This slow rise in the  $\alpha$ -C<sub>2</sub>SH phase shows the impact of retardation in the Class G + R sample. The class G (control) sample displayed

a drastic decrease in  $\alpha$ -C<sub>2</sub>SH after 5.2 hours of hydration, while at the same time this was accompanied by an increase in 11 Å tobermorite (see Figure 3C). After 10 hours of hydration the Class G + R sample showed an initial decrease in  $\alpha$ -C<sub>2</sub>SH but always maintained higher  $\alpha$ -C<sub>2</sub>SH values compared to the Class G sample.  $\alpha$ -C<sub>2</sub>SH concentration dropped as the crystalline component of the cement paste converted to 11 Å tobermorite. At the early stage of hydration, a direct correlation between  $\alpha$ -C<sub>2</sub>SH and 11 Å tobermorite cannot be attributed since multiple hydration paths are occurring, which could affect the formation of these phases. The UCA was used to estimate the compressive strength of the cement as a function of time and to relate compressive strength to the XRD information.

The UCA was used to examine the compressive strength effect during hydration by maintaining similar pressure and temperature conditions as the XRD data experiment (refer to Figure 5). The data from the UCA are representative of cement's suitability under downhole conditions. Throughout the hydration time, the Class G sample showed higher compressive strength compared to the Class G + R sample. An initial increase in compressive strength was observed after 1.6 and 7.3 hours for the Class G and Class G + R samples, respectively. It is worth noting that the time for the strength increase in the Class G sample corresponds to the increase in the 11 Å tobermorite phase (see Figure 3C). The evolution of the 11 Å tobermorite phase started around 1.8 hours for the Class G sample, which suggests that 11 Å tobermorite was responsible for the strength increase in these cement pastes. The Class G + R sample showed a drastic increase in the 11 Å tobermorite phase between 7 and 12 hours, which corresponds to the increase in compressive strength at 7.3 hours as shown by the UCA data (see Figure 5B). The maximum strength gain of 11.73 and 9.54 MPa was detected for the Class G and Class G + R samples, respectively. Although 11 Å tobermorite helped to increase the compressive strength, a simultaneous increase in  $\alpha$ -C<sub>2</sub>SH led to a reduction in compressive strength. Careful engineering of these phases is required to

examine the strength impact when retarders are used with oil well cements under realistic conditions.

In situ XRD revealed the phases that influenced the retardation process throughout the hydration. The delay effect was observed by a change in the rate of the appearance of 11 Å tobermorites as well as a change in the rate of the  $\alpha$ -C<sub>2</sub>SH generation and depletion. In the cement hydration process, water conversion from free to bound water hardens the cement paste. Examination of the physiochemical properties of the water during hydration facilitates monitoring of the reaction kinetics and structural dynamics that are responsible for the strength gain accompanied by nucleation and growth of the hydration products. Next, we evaluate the effect of water dynamics on hydrating oil well cements using QENS techniques under similar temperature and pressure conditions that were used for the synchrotron XRD experiment.

## 3.2 | Quasielastic neutron scattering

### 3.2.1 | Modeling QENS data

During cement hydration, hydrogen from the water component combines with the binder to form hydration products. QENS can detect the water regardless of the crystalline or amorphous component of the binder matrix.<sup>30</sup> QENS provides information about the water dynamics of the material because of the energy exchange between an incident and scattered neutrons as an outcome of interacting with the sample.<sup>31</sup> The QENS response to hydrating the cement paste involves a scattering due to the diffusion of atoms, resulting in broadening caused by the energy change imparted by the neutrons from the moving hydrogen nuclei.<sup>18</sup> The broadened peak is fitted via a Lorentzian distribution. Additionally, the peak width of the water component is influenced by the presence of solid interfaces, which constricts the water inside the gel pores. The bound hydrogen atoms are represented by a sharp peak centered on the neutron energy since the scattering is elastic and is fitted using a Gaussian distribution.

The QENS data were modeled using data analysis and visualization environment software.<sup>32</sup> The QENS energy transfer spectrum,  $S(Q, \omega)$  was modeled using the background term  $C_0$ , which is the fixed baseline intensity;  $P$  represents the scattered elastic intensity relating to the number density of CB water;  $B_1$  is the number density of free hydrogen atoms representing the bulk water component, while  $\Gamma_1$  is the fixed Lorentzian half-width-half-maximum (HWHM) for the bulk water component;  $B_2$  is the number density of hydrogen atoms in constrained form, while  $\Gamma_2$  is the variable Lorentzian HWHM for the constrained water component.<sup>33</sup> A vanadium standard was used to measure the instrument resolution, where  $\sigma$  reflects the Gaussian standard deviation of the measured resolution function of the spectrometer.

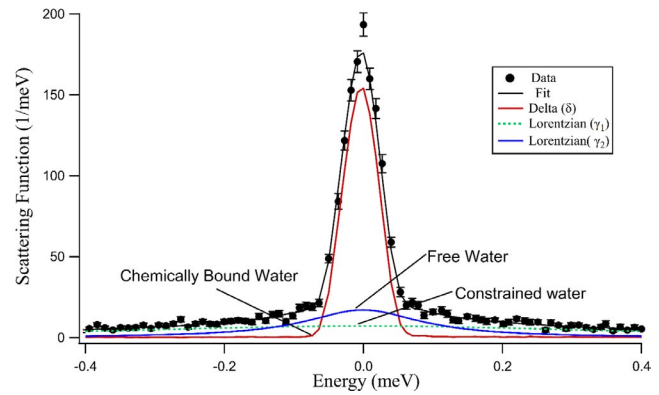


**FIGURE 6** Typical fit of the quasielastic neutron scattering data after 30 min of hydration for the Class G + 3R sample [Color figure can be viewed at [wileyonlinelibrary.com](http://wileyonlinelibrary.com)]

$$S(Q, \omega) = C_0 + \left( P[\delta(\omega=0)] + B_1 \left[ \frac{\Gamma_1}{\pi(\Gamma_1^2 + \omega^2)} \right] + B_2 \left[ \frac{\Gamma_2}{\pi(\Gamma_2^2 + \omega^2)} \right] \right) \otimes \left( \frac{e^{-\omega^2/2\sigma^2}}{\sigma\sqrt{2\pi}} \right). \quad (1)$$

A sample fit of the QENS data for the retarder sample (Class G + 3R) after 30 minutes of hydration is shown in Figure 6. The red line represents the elastic contribution by the Gaussian intensity, the solid black line represents the total fit of the data, and the blue and green lines represent the free water and constrained water Lorentzian functions, respectively.

The bound water index (BWI) was calculated using Equation (1) above, where BWI represents the relative amount of immobile hydrogen atoms.

$$\text{BWI} = \frac{P_A + B_{2A}}{P_A + B_{1A} + B_{2A}}. \quad (2)$$

In Equation (2) above,  $P_A$ ,  $B_{1A}$ , and  $B_{2A}$  are the areas under Gaussian ( $P$ ) and the two Lorentzians ( $B_1$  and  $B_2$ ).  $P_A + B_{2A}$  represents the total bound water in the hydrating paste. This model facilitates three populations of hydrogen including immobile hydrogen in cement paste ( $P$ ), freely diffusing water ( $\Gamma_1$ ), and constrained water ( $\Gamma_2$ ) in the hydrating cement paste as a function of time.

The completely bound index (CBI) and constrained water index (CWI) were calculated by the formula below<sup>33</sup>:

$$\text{CBI} = \frac{P_A}{P_A + B_{1A} + B_{2A}}, \quad (3)$$

$$\text{CWI} = \frac{B_{2A}}{P_A + B_{1A} + B_{2A}}. \quad (4)$$

The CBI examines the impact of the Gaussian component, which is the elastic response of the chemically bound water, whereas the CWI considers only the area under the

constrained water Lorentzian. Sole evaluation of constrained water is essential as the evolution of the constrained water inside the confined region (gel pores) leads to the initiation of the hardening process accompanied by an increase in the total surface area of the hydration products.

### 3.2.2 | Tracking in situ hydration via QENS

A three-dimensional plot of the QENS spectra for hydrating cement paste throughout 43 hours for a Class G + 3R sample is shown in Figure 7A. For each QENS spectrum, the data were summed over all  $Q$  values from 0.1 to 2  $\text{\AA}^{-1}$ . The hydration reaction is commenced when the water reacts with the cementitious binder resulting in the conversion of free water to chemically bound water due to the formation of hydration products. A distinct feature is the steady rise of elastic intensity with the increase in the hydration time. The broadening effect in the quasielastic spectrum is attributed to the reduction in free water, and the increase in elastic intensity is related to the formation of C–S–H and other related crystalline phases.<sup>19,34</sup> Stabilization of elastic intensity is an indication of initiation of setting; however, a slight movement of water has been observed among mature cement pastes, thus stabilization of elastic intensity is not a direct measure of the setting time of the cement paste.<sup>35</sup>

Motions arising from bulk water were examined by plotting  $S(Q, \omega)$  against the scattering vector ( $Q$ ) values after 135 minutes of hydration (Figure 7B). As the  $Q$  values increase, the broadening of the QENS spectra is observed indicating that the motions are diffusive and are originating

from the free water component. Additionally, at various  $Q$  values, different diffusive motions occur and, usually, widths are proportional to the  $Q^2$  of the Lorentzians.<sup>20</sup> Here, the energy spectrum of the scattered neutrons indicates the shape of the Lorentzian functions whose half-width-half-maximum (HWHM) increases with momentum transfer.<sup>36</sup>

In what follows, we calculate the bound water index (BWI) using Equation (1) to investigate the effect of retardation on Class G cement pastes at elevated temperature and pressure conditions.

### 3.2.3 | Bound water index

The impact of immobile water on hydration was examined by calculating the BWI values for Class G and Class G + 3R samples (Figure 8A,C). A BWI value of 0 represents free water and no presence of mobile components of water; while a value of 1 means no free water is available and the cement paste is in the hardened stage. The first rise in BWI was detected after 1 and 2 hours of hydration for Class G and Class G + 3R samples, respectively (Figure 8C). This initial rise in BWI values correlate with the compressive strength data obtained from the UCA. From the UCA data, the Class G and Class G + 3R samples showed an initial strength increase after 1.5 hours and 2.6 hours, respectively. The class G sample indicated a second sharp increase in BWI after 3.75 hours of hydration, while the Class G + 3R sample showed the second rise after 12 hours. The second rise in BWI after 3.75 hours matches the transition at 3.5 hours from the UCA data

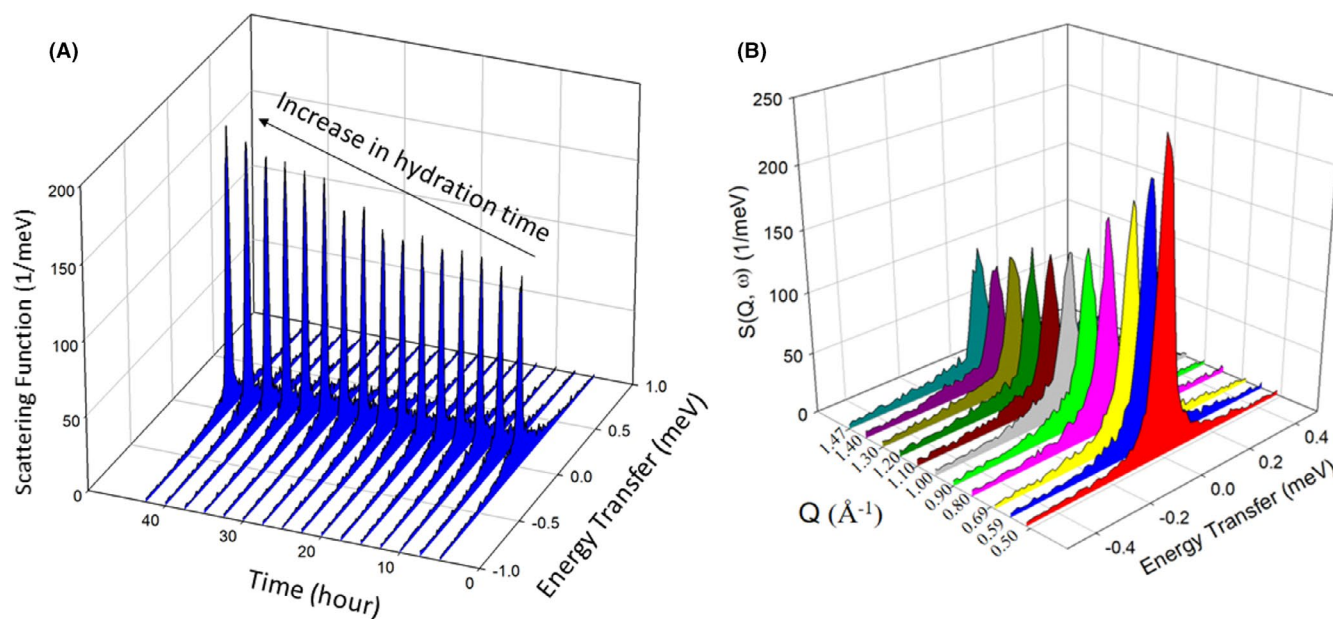


**FIGURE 7** A, Three-dimensional plot of the quasielastic neutron scattering (QENS) spectra for hydrating cement paste for 43 h for the Class G + 3R sample. B,  $Q$ -dependence analysis for the QENS spectra on the Class G + 3R sample indicating broadening with increase in  $Q$  values [Color figure can be viewed at [wileyonlinelibrary.com](http://wileyonlinelibrary.com)]

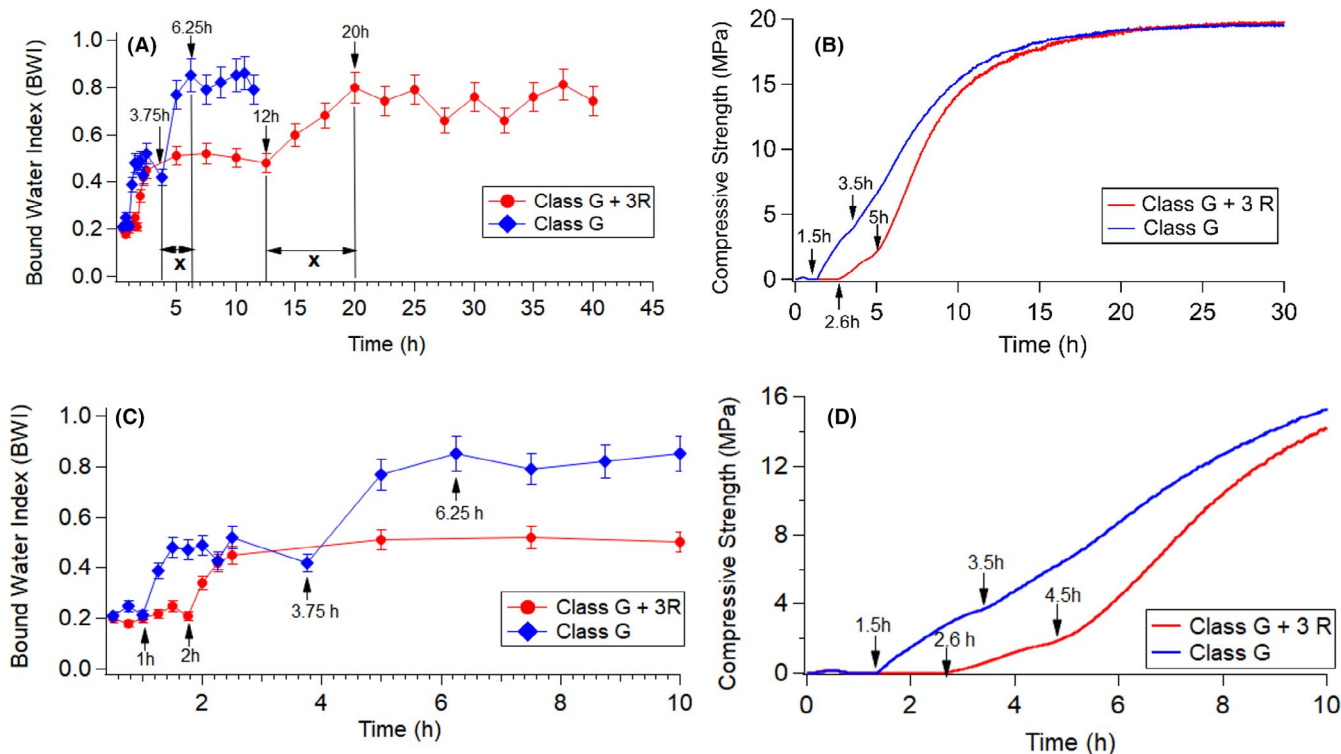


**FIGURE 8** A, Bound water index (BWI) data for the first 45 h showing the retarder effect. B, Corresponding ultrasonic cement analyzer (UCA) data collected under similar pressure and temperature conditions. C, Zoomed images of BWI. D, UCA data for the first 10 h of hydration [Color figure can be viewed at [wileyonlinelibrary.com](http://wileyonlinelibrary.com)]

showing a two-tiered strength development (Figure 8C,D). The two-tiered strength development is common when DTPMP-based retarders are used with oil well cements, and the confluence of water dynamics can be observed with a slight dip in the BWI values at the transition point. The Class G sample showed a sharp rise in BWI values from 0.42 at 3.5 hours to 0.85 at 6.2 hours, whereas the Class G + 3R sample showed a noticeable increase in BWI after 12 hours from 0.48 to 0.8 at 20 hours (Figure 8A). This increase is marked as *x*, showing the effect of retarder on the actual times when a steady rise in BWI values was observed for samples with and without retarders.

The BWI is also a measure to evaluate the retardation of nucleation and growth kinetics, which is limited by the diffusion of water into the growing phases.<sup>30</sup> The Class G sample showed tapering of the BWI values around 6.25 hours, while this tendency was detected after 20 hours for the Class G + 3R sample (Figure 8A). In the presence of retarder, the initiation of nucleation and growth phases was more gradual because of the slow rate of conversion from free water to chemically or constrained water components. This trend can be related to the slower setting time leading to a delay in the growth of the phases, which is influenced by the retarder. This feature can be related to the slow growth evolution of the 11 Å tobermorite phase due to the influence of the retarder inhibiting the strength increase in the cement paste.

In addition to the BWI, QENS measurements of hydrating cement paste can discern the effect of completely bound and constrained water. From QENS<sup>33</sup> and Small Angle Neutron Scattering<sup>37,38</sup> studies, we know that the constrained water is detected on the surface of the hydration product. The influence of retarders on completely bound (structural water) and constrained water is shown in Figure 9A,B, respectively. The Class G sample displayed a steady rise in the CBI values throughout hydration (Figure 9A). In contrast, the Class G + 3R sample maintained CBI values of 0.28–0.34 between 3.6 and 30 hours. After 30 hours, the Class G + 3R sample showed a rise in CBI values from 0.34 to 0.52. Completely bound or structural water is associated with the formation of the C–S–H-based systems.<sup>39</sup> The control sample (Class G) showed a steady rise in the structural water component, while the retarder sample (Class G + 3R) had a gradual growth of structural water, suggesting delayed development of the hydration phases. Furthermore, at the early stage of curing, fast filling of capillary pores occurs which indicates the evolution of the structural water component in forming the C–S–H and calcium hydroxide phases. Hence, by retarding the growth of structural water, the phosphonate-based retarder delayed the rapid pore-filling process and thus prevented the hardening of the cement paste. Next, we evaluate retardation by analyzing only the constrained water population by CWI analysis.

The control sample (Class G) showed higher CWI values compared to the Class G + 3R sample (see Figure 9B).

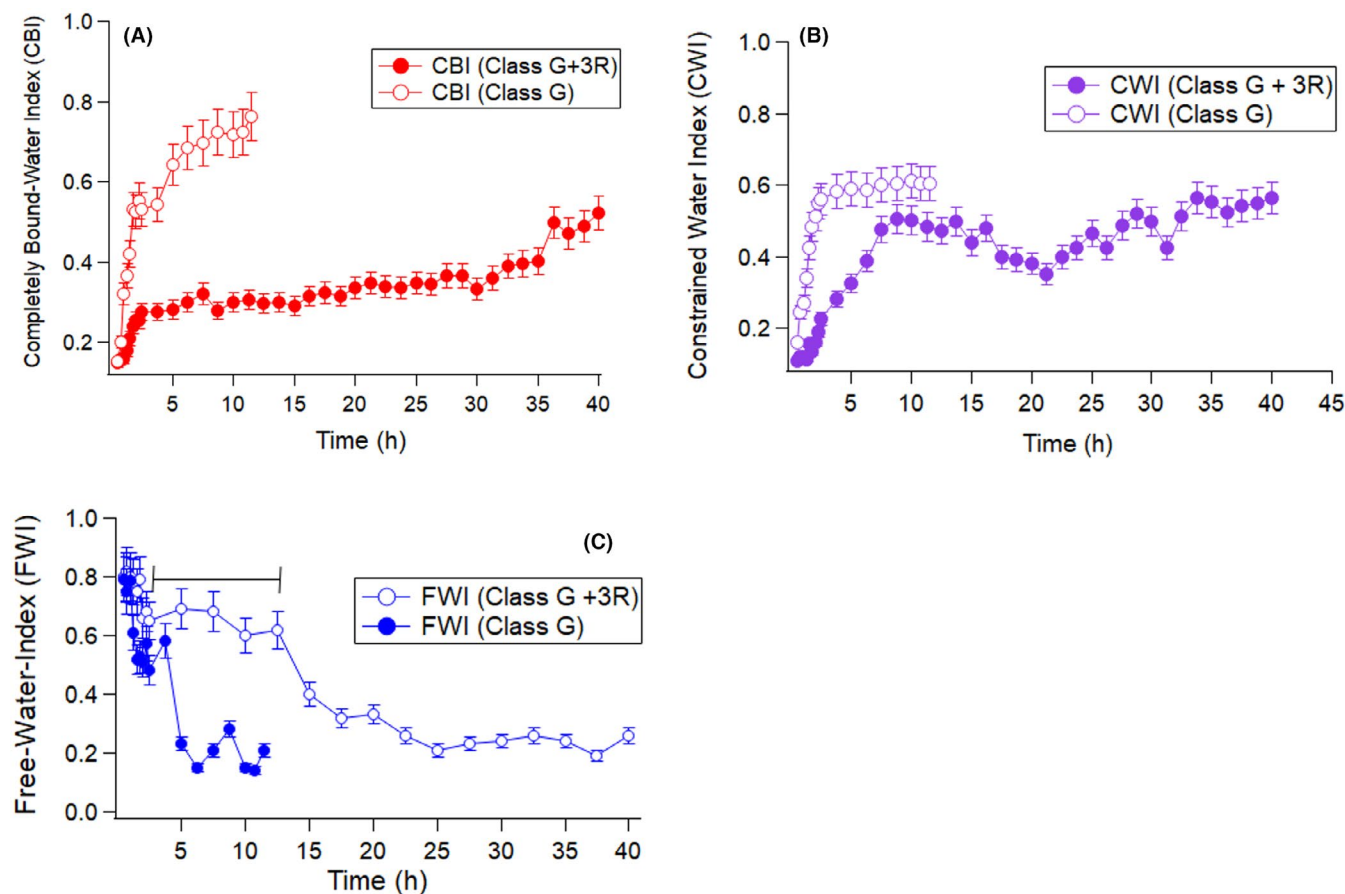


**FIGURE 9** A, Completely bound water index (CBI) and (B) constrained water index showing the retarder effect on gel pores. (C) Hydration kinetics measured via free water index (FWI) analysis [Color figure can be viewed at [wileyonlinelibrary.com](http://wileyonlinelibrary.com)]

The Class G sample showed a sharp rise in CWI values up to 4 hours of hydration, while the retarder sample had a more gradual increase in CWI values up to 10 hours. For the Class G + 3R sample, no sharp rise in CWI values was detected between 10 and 20 hours of curing. After 20 hours, the second increase in CWI values was observed up to 35 hours before leveling off. The apparent effect of retardation was detected between 10 and 20 hours of hydration because of the limited growth of the constrained water population.

Based on the CWI analysis during the initial 1 hour of hydration, there was no steady rise in CWI values, suggesting no well-defined pore structure. The amount of constrained water can be associated with the total surface area of the hydration products.<sup>17</sup> The kinetics of constrained water suggest a relationship to the development of the specific surface area of the cement paste. The specific surface area of the cement paste increases rapidly during the early hours of hydration where the initial rapid filling of the capillary pores occurs. As the constrained water starts to level off, the gel pore filling follows. Lower values of constrained water suggest the amount of C–S–H is less since in the early age of curing and the formation of C–S–H originates entirely from  $C_3S$  consumption. These results correlate the XRD results, where the

retarder prevents the rapid consumption of  $C_3S$  by arresting the growth of portlandite and 11 Å tobermorite formation. The constrained water intensity rises rapidly during the first few hours of hydration before leveling off (Figure 9B). In contrast, the structural water (completely bound) intensity increases but does not level off immediately (Figure 9A). Moreover, the completely bound or structural water follows the heat of evolution, while the constrained water does not follow this trend.<sup>18</sup> In the presence of a retarder, the structural water levels off, indicating slower nucleation and growth of the phases. Thus, this work shows that retardation of structural or completely bound water is necessary for delaying the hardening and setting of the cement paste.

The free water index (FWI)<sup>33</sup> is calculated by 1-BWI (see Figure 9C). In comparison to the control sample (Class G), the FWI values were much higher for the Class G + 3R sample. As the cement paste hydrates, the width of the free water Lorentzian peak decreases, initiating the drop in FWI values. For the first 2 hours, both the samples showed a drop in FWI values from 0.82 to 0.66. After 2.5 hours the retarder sample was able to maintain FWI values between 0.75 and 0.65 for up to 12.5 hours while the control sample (Class G) exhibited a continuous drop in FWI from 0.58 to 0.23 between

4 and 5 hours of hydration. The plateau between 2.5 and 12.5 hours for the Class G + 3R sample corresponds to an induction time during which hydrogen density appears to be constant (Figure 9C). In this period the remaining fraction of water molecules are in the transition process of forming new phases.<sup>40</sup> The presence of free water is an indication of a dormant period where conversion from free to chemically bound water is retarded. Thus, from CBI, CWI, and FWI analysis, we can conclude that the retarder has a predominant effect on the free and structural water component, thus delaying the overall setting of the cement paste.

The free water regime mostly impacts the capillary pore structure, while the constrained water component is detected in the gel pores.<sup>24</sup> A highly reactive C–S–H surface stimulates hydrolytic reactions at the solid/liquid interface, which initiates the transformation of Si–OH and Ca–OH chemical groups to be infused in the C–S–H structure. During this reaction, the hydrogen bonds are linked to Ca–OH and Si–OH groups, thus restricting the mobility of the surface water molecules inside the C–S–H phase. Next, we evaluate the dependence of the broadening as a function of  $Q$  which provides detailed information related to the type of motion, such as free diffusion, random jump-diffusion, and diffusion inside the confined region.<sup>31,36</sup> It must be noted that when  $Q$  is less than approximately  $1.4 \text{ \AA}^{-1}$ , only contributions from the translational motion of water are considered.<sup>41</sup>

The  $Q$  dependence of HWHM ( $\Gamma$ ) of the constrained water Lorentzian at different  $Q$  values is shown in Figure 10. Typically, Lorentzian functions show  $Q$  dependence with confinement environments inside cementitious materials.<sup>40</sup> In comparison to the Class G + 3R sample, the HWHM values obtained from constrained water Lorentzian were higher for the Class G sample. In Figure 10, we observe that with a low  $Q$  value, the Lorentzian is flat with constant values referring to water confinement in the restricted area. Under the confined regime, the water mobility will shift to longer relaxation times

during the bulk water process; meanwhile, the water enclosed in the large capillary pores acts as “bulk-like.”<sup>42</sup> This confinement regime occurs during the early stage of the hydration process during the evolution of the initial reaction products. As the  $Q$  values increase, the dominance of bulk diffusion inside the confinement region is regained. The dashed lines represent this transition at  $Q$  values initiating the process when restricted water-to-bulk diffusion occurs in the confined region. As the hydration reaction proceeds, the flattened line became shorter and a steady increase in the HWHM values was observed at lower  $Q$  values. For instance, after 30 minutes of hydration, the Class G + 3R sample displayed nearly a flat line indicating no constrained water, whereas a jump in HWHM value at  $Q = 1.1$  can be detected after 2 hours of hydration (Figure 10B). The control (Class G) sample showed a rise in Lorentzian values even after 30 minutes of hydration (Figure 10A). As the hydration time increased, the rise in HWHM values was observed at low  $Q$  values, suggesting diffusive movement where free water is getting converted to constrained water. Thus, the retarder was able to slow the dominance of bulk diffusion in the restricted area where the confined water was not completely involved in the nucleation and growth of the hydration phases. The entrapped constrained water can also contribute to the growth of the hydration products leading to enhanced strength in the binding gel. Thus, restricting the constrained water in the gel pores infers to slower growth of the C–S–H and Portlandite phase.

This work examined oil well cement hydration in the presence of retarders using realistic downhole conditions considering the simultaneous effect of pressure and temperature conditions. The benefit of using in situ measurements simulating downhole conditions is to evaluate the phase changes as well as decipher the water population environment, which is responsible for the phase changes during the hydration. To date, the majority of research on oil well cements is done in local laboratory settings where real-time tracking of cementing under

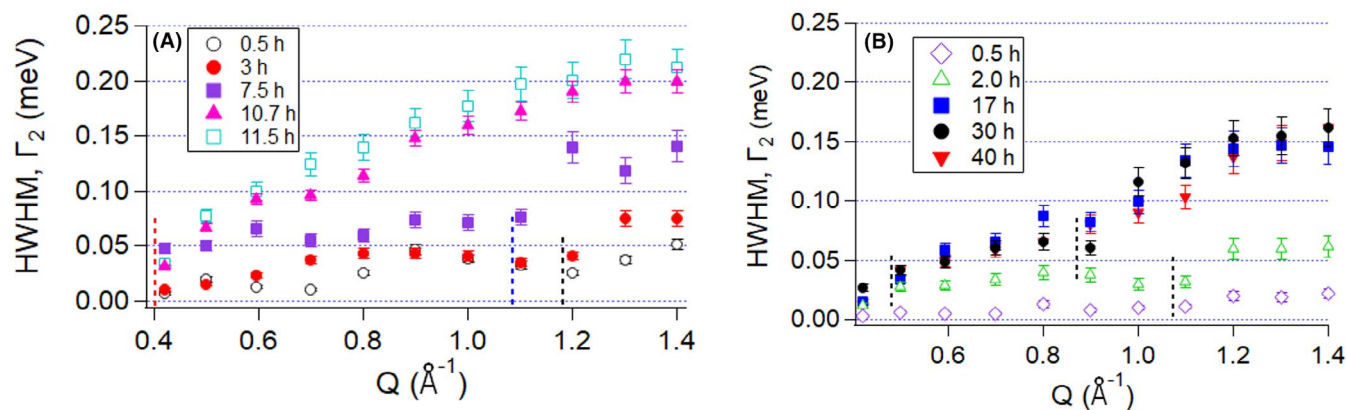


**FIGURE 10** Half-width-half-maximum (HWHM) of the constrained Lorentzian component vs momentum transfer ( $Q$ ) for (A) Class G (control) and (B) Class G + 3R (with retarder) sample. The dashed line represents a guide to locate  $Q$  values [Color figure can be viewed at [wileyonlinelibrary.com](http://wileyonlinelibrary.com)]

elevated temperature/pressure conditions is difficult. Thus, the use of advanced X-ray synchrotron and neutron-based techniques will facilitate real-time tracking which, in turn, will help engineer retarders for downhole conditions.

## 4 | CONCLUSIONS

Quasielastic neutron scattering and synchrotron-based XRD were used to investigate the retardation effect in oil well cement pastes at elevated temperature and pressure conditions. From this work, we showed that both water dynamics and microstructure analysis are required to understand the holistic effect on retardation in oil well cement hydration. Results from XRD and QENS were related to the strength values obtained from the UCA.

From the XRD results, the retardation effect was observed by slower formation of 11 Å tobermorites and a delay in the observed  $\alpha$ -C<sub>2</sub>SH dynamics. The retarder tested slowed down the hydration of crystalline C<sub>3</sub>S by delaying the growth rate of 11 Å tobermorite and portlandite phases. A slower rate of increase in the 11 Å tobermorite phase corresponds to a delayed increase in compressive strength. In the presence of the retarder, the conversion of 11 Å tobermorite to  $\alpha$ -C<sub>2</sub>SH phase also led to a decrease in compressive strength.

Quasielastic neutron scattering studies were performed to evaluate the impact of retarder on free, structural (completely bound), and constrained water populations. Water dynamics studies showed that the retarder was successful in decreasing the bounding capacity of water by lowering the BWI values when compared to the control sample. Due to the retardation effect, initiation of nucleation and growth phases was more gradual, slowing the rate of conversion from free water to chemically or constrained water components. At the early age of hydration, phosphonate-based retarders were successful in impeding the growth of structural water components by delaying the rapid pore-filling process, thus preventing the setting of the cement paste. As a result of retardation, lower values of the constrained water index are related to the decreased amount of C–S–H, especially 11 Å tobermorite, which led to the decrease in the compressive strength of cement paste. Here, we showed that retardation of structural or completely bound water is necessary for delaying the hardening and setting of the cement paste.

From *Q* dependence analysis, the retarder was able to slow the dominance of bulk diffusion in the restricted area, where the confined water was not involved in the nucleation and growth of the hydration phases. Over the temperature/pressure interval, multiple hydration paths arise, and a strong influence of water dynamics impacts the retardation process. Free water analysis is critical to determine the induction periods, which can be corroborated by the UCA data. Thus, QENS is a valuable tool to accurately detect the lag or induction period due to retardation effect.

## ACKNOWLEDGMENTS

We thank Aramco Services Company (ASC) for funding this research. Use of the Advanced Photon Source at Argonne National Laboratory was supported by the US Department of Energy, Office of Science, Office of Basic Energy Sciences, under contract no. DE-AC02-06CH11357. Access to the disk chopper spectrometer was provided by the Center for High Resolution Neutron Scattering, a partnership between the National Institute of Standards and Technology and the National Science Foundation under agreement no. DMR-1508249. We acknowledge the support of the National Institute of Standards and Technology (NIST), US Department of Commerce for providing the neutron research facilities used in this work. We acknowledge the help and support of Dr. Nicholas P. Butch and Dr. Madhusudan Tyagi from NCNR during the QENS measurements at NIST. This work made use of the Shared Experimental Facilities supported in part by the MRSEC Program of the National Science Foundation under award number DMR-1419807. We thank Dr. Charles Settens from the Massachusetts Institute of Technology Material Research Laboratory (MRL) for his assistance in the XRD data analysis. Finally, we would like to especially thank Dr. Ashraf Al-Tahini, Director of ASC for his encouragement and support during this work.

## ORCID

Kunal Kupwade-Patil  <https://orcid.org/0000-0002-7166-8257>

Oral Büyükköztürk  <https://orcid.org/0000-0002-7712-7478>

## REFERENCES

- Nelson EB, Guillot D. Well cementing. Sugar Land, Texas: Schlumberger; 2006.
- Nelson EB, Michaux M, Drochon B. Cement additives and mechanisms of action. In: Nelson EB, Guillot D, editors. Well cementing. Sugar Land, TX: Schlumberger; 2006. p. 49–91.
- Cheung J, Jeknavorian A, Roberts L, Silva D. Impact of admixtures on the hydration kinetics of portland cement. *Cem Concr Res*. 2011;41(12):1289–309.
- Kupwade-Patil K, Boul PJ, Rasner DK, Everett SM, Proffen T, Page K, et al. Retarder effect on hydrating oil well cements investigated using in situ neutron/X-ray pair distribution function analysis. *Cem Concr Res*. 2019;126:105920.
- Boul PJ, Rasner DK, Johnson KD, Thaemlitz CJ. The impact of powerful retarding additive synergies on the kinetic profile of cementitious mineralogical transformations at high temperature. *MRS Commun*. 2019;9(3):1022–8.
- Pang X, Boontheung P, Boul PJ. Dynamic retarder exchange as a trigger for Portland cement hydration. *Cem Concr Res*. 2014;63:20–8.
- Jupe AC, Wilkinson AP, Luke K, Funkhouser GP. Class H cement hydration at 180°C and high pressure in the presence of added silica. *Cem Concr Res*. 2008;38(5):660–6.
- Jupe AC, Wilkinson AP, Luke K, Funkhouser GP. Class H oil well cement hydration at elevated temperatures in the presence of retarding agents: an in situ high-energy X-ray diffraction study. *Ind Eng Chem Res*. 2005;44(15):5579–84.
- Colston SL, Barnes P, Jupé AC, Jacques SDM, Hall C, Livesey P, et al. An in situ synchrotron energy-dispersive diffraction study of the

- hydration of oil well cement systems under high temperature/autoclave conditions up to 130°C. *Cem Concr Res.* 2005;35(12):2223–32.
10. Jupe AC, Wilkinson AP, Luke K, Funkhouser GP. Slurry consistency and in situ synchrotron X-ray diffraction during the early hydration of Portland cements with calcium chloride. *J Am Ceram Soc.* 2007;90(8):2595–602.
  11. Taylor HFW. *Cement chemistry*. 2nd ed. London, UK: Thomas Telford; 1997.
  12. Jupe AC, Wilkinson AP, Funkhouser GP. The effect of pressure on tricalcium silicate hydration at different temperatures and in the presence of retarding additives. *Cem Concr Res.* 2012;42(8):1083–7.
  13. Peterson VK, Neumann DA, Livingston RA. Hydration of tricalcium and dicalcium silicate mixtures studied using quasielastic neutron scattering. *J Phys Chem B.* 2005;109(30):14449–53.
  14. Peterson VK, Juenger MCG. Hydration of tricalcium silicate: effects of CaCl<sub>2</sub> and sucrose on reaction kinetics and product formation. *Chem Mater.* 2006;18(24):5798–804.
  15. Peterson VK, Neumann DA, Livingston RA. Inelastic neutron scattering investigation of hydrating tricalcium and dicalcium silicate mixture pastes: Ca(OH)<sub>2</sub> formation and evolution of strength. *J Mater Res.* 2006;21(07):1836–42.
  16. Peterson VK, Brown CM, Livingston RA. Quasielastic and inelastic neutron scattering study of the hydration of monoclinic and triclinic tricalcium silicate. *Chem Phys.* 2006;326(2–3):381–9.
  17. Gutberlet T, Hilbig H, Beddoe RE, Lohstroh W. New insights into water bonding during early tricalcium silicate hydration with quasielastic neutron scattering. *Cem Concr Res.* 2013;51:104–8.
  18. Thomas JJ, FitzGerald SA, Neumann DA, Livingston RA. State of water in hydrating tricalcium silicate and Portland cement pastes as measured by quasi-elastic neutron scattering. *J Am Ceram Soc.* 2001;84(8):1811–6.
  19. Berliner R, Popovici M, Herwig KW, Berliner M, Jennings HM, Thomas JJ. Quasielastic neutron scattering study of the effect of water-to-cement ratio on the hydration kinetics of tricalcium silicate. *Cem Concr Res.* 1998;28(2):231–43.
  20. Kupwade-Patil K, Tyagi M, Brown CM, Büyükköztürk O. Water dynamics in cement paste at early age prepared with pozzolanic volcanic ash and ordinary Portland cement using quasielastic neutron scattering. *Cem Concr Res.* 2016;86:55–62.
  21. Kupwade-Patil K, Bumajdad A, Brown CM, Tyagi M, Butch NP, Jamsheer AF, et al. New insights into water dynamics of Portland cement paste with nano-additives using quasielastic neutron scattering. *J Mater Sci.* 2019;54(6):4710–8.
  22. Kupwade-Patil K, Diallo SO, Hossain DZ, Islam MR, Allouche EN. Investigation of activation kinetics in geopolymer paste using quasielastic neutron scattering. *Constr Build Mater.* 2016;120:181–8.
  23. Gong K, Cheng Y, Daemen LL, White CE. In situ quasi-elastic neutron scattering study on the water dynamics and reaction mechanisms in alkali-activated slags. *Phys Chem Chem Phys.* 2019;21(20):10277–92.
  24. Hou D, Li Z, Zhao T, Zhang P. Water transport in the nano-pore of the calcium silicate phase: reactivity, structure and dynamics. *Phys Chem Chem Phys.* 2015;17(2):1411–23.
  25. Degen T, Sadki M, Bron E, König U, Nénert G. The HighScore suite. *Powder Diffr.* 2014;29(S2):S13–S18.
  26. Institute AP. American Petroleum Institute RP 10B: recommended practice for testing well cements. Washington, DC: API; 2013. p. 124.
  27. Bresson B, Meducin F, Zanni H, Noik C. Hydration of tricalcium silicate (C<sub>3</sub>S) at high temperature and high pressure. *J Mater Sci.* 2002;37(24):5355–65.
  28. Marchon D, Flatt RJ. Impact of chemical admixtures on cement hydration. In: Aitcin P, Flatt RJ, editors. *Science and technology of concrete admixtures*. Cambridge, UK: Woodhead Publishing; 2016. p. 279–304.
  29. Bullard JW, Flatt RJ. New Insights Into the effect of calcium hydroxide precipitation on the kinetics of tricalcium silicate hydration. *J Am Ceram Soc.* 2010;93(7):1894–903.
  30. Peterson V. Studying the hydration of cement systems in real-time using quasielastic and inelastic neutron scattering. In: Eckold G, Schober H, Nagler SE, editors. *Studying kinetics with neutrons*. Springer Series in Solid-State Sciences. Berlin/Heidelberg, Germany: Springer; 2010;161:p. 19–75.
  31. Hempelmann R. Quasielastic neutron scattering and solid state diffusion. Oxford, UK: Oxford University Press; 2000.
  32. Azuah RT, Kneller LR, Qiu Y, Tregenna-Piggott PLW, Brown CM, Copley JRD, et al. DAVE: a comprehensive software suite for the reduction, visualization, and analysis of low energy neutron spectroscopic data. *J Res Natl Inst Stand Technol.* 2009;114(6):341–58.
  33. Allen AJ, McLaughlin JC, Neumann DA, Livingston RA. In situ quasi-elastic scattering characterization of particle size effects on the hydration of tricalcium silicate. *J Mater Res.* 2004;19(11):3242–54.
  34. Berliner R, Popovici M, Herwig K, Jennings HM, Thomas J. Neutron scattering studies of hydrating cement pastes. *Physica B Condens Matter.* 1997;241-243:1237–9.
  35. Bordallo HN, Aldridge LP, Desmedt A. Water dynamics in hardened ordinary Portland cement paste or concrete: from quasielastic neutron scattering. *J Phys Chem B.* 2006;110(36):17966–76.
  36. Bée M. *Quasielastic neutron scattering*. Bristol, England: Adam Hilger. 1988.
  37. Thomas JJ, Chen JJ, Allen AJ, Jennings HM. Effects of decalcification on the microstructure and surface area of cement and tricalcium silicate pastes. *Cem Concr Res.* 2004;34(12):2297–307.
  38. Allen AJ, Thomas JJ, Jennings HM. Composition and density of nanoscale calcium-silicate-hydrate in cement. *Nat Mater.* 2007;6(4):311–6.
  39. Nemes NM, Neumann DA, Livingston RA. States of water in hydrated C<sub>3</sub>S (tricalcium silicate) as a function of relative humidity. *J Mater Res.* 2006;21(10):2516–23.
  40. Viani A, Zbiri M, Bordallo HN, Gualtieri AF, Mácová P. Investigation of the setting reaction in magnesium phosphate ceramics with quasielastic neutron scattering. *J Phys Chem C.* 2017;121(21):11355–67.
  41. Fratini E, Chen S-H, Baglioni P, Bellissent-Funel M-C. Quasi-elastic neutron scattering study of translational dynamics of hydration water in tricalcium silicate. *J Phys Chem B.* 2002;106(1):158–66.
  42. Jacobsen J, Rodrigues MS, Telling MTF, Beraldo AL, Santos SF, Aldridge LP, et al. Nano-scale hydrogen-bond network improves the durability of greener cements. *Sci Rep.* 2013;3:2667.

**How to cite this article:** Kupwade-Patil K, Boul PJ, Rasner DK, et al. In situ investigation of phosphonate retarder interaction in oil well cements at elevated temperature and pressure conditions. *J Am Ceram Soc.* 2020;103:6400–6413. <https://doi.org/10.1111/jace.17373>